Experimental Test of Baryon Conservation and Neutrino Flux Limits*

W. R. KROPP, JR.† AND F. REINES
Case Institute of Technology, Cleveland, Ohio
(Received 3 August 1964)

An experiment has been performed in which events not directly attributable to cosmic rays or natural radioactivity were observed for 4500 h in a 200-liter liquid scintillation detector. Shielding from cosmic rays was obtained through anticoincidence techniques and by locating the detector 585 m underground. Background from natural radioactivity was reduced by placing high-energy requirements on acceptable events. The residual signal has been used to establish new lower limits on the stability of nucleons and a new upper limit on the product of the cross section and the electron neutrino (ν_e,$\bar{\nu}_e$) flux whatever its origin, providing its energy is <400 MeV and >30 MeV (ν_e) or >12 MeV($\bar{\nu}_e$). Depending on the assumed decay modes, nucleon lifetime limits in the range 0.6×10^{28} to 4×10^{28} years were obtained. The upper limits on the neutrino cross-section flux products are $<8.5\times10^{-38}$ ν_e sec^{-1} and $<3.2\times10^{-38}$ $\bar{\nu}_e$ sec^{-1}.

INTRODUCTION

ALL theories of elementary particles assume the validity of the law of conservation of baryons; i.e., that the number of baryons minus the number of antibaryons is constant in any interaction. The baryons are all those fermions with mass greater than or equal to that of the proton. In its earliest form the principle was discussed by Stückelberg[1] and Wigner[2] as a conservation law for nucleons: they do not decay spontaneously, nor are they created, except in nucleon-antinucleon pairs.

It is interesting that within the realm of the known elementary particles, violation of this conservation law cannot occur unless one or more of the conservation laws of energy-momentum, charge, spin or lepton number is also violated. Taking lepton conservation as the least well founded, decay modes violating this principle were considered (Table I).

A number of experiments[3–6] have tested the validity of nucleon conservation by investigating the stability of nucleons against spontaneous decay. The results of the present experiment have been used to establish more stringent lower limits on the nucleon lifetime than those previously reported. The technique is essentially that of Giamati and Reines[5] whose equipment was modified for the present work.

The experiment consisted of the search for events in a shielded liquid scintillation detector (the inner detector of Fig. 1). If the observed events are ascribed to decaying nucleons in the detector and its environment, lifetime limits can be established. The cosmic-ray background was reduced from the unshielded sea-level value by $\sim7\times10^7$ by placing the liquid scintillation detector 585 m underground in a salt mine and enclosing it in an anticoincidence guard. Background from natural radioactivity was eliminated by requiring that acceptable events deposit at least 9 or 10 MeV in the inner detector.

An interpretation of the data in terms of the cosmic-ray neutrino flux is also presented. In this interpretation the iron shielding is viewed as a source of target nucleons for the incident neutrinos.

Reactions of the type

$$\bar{\nu}_e^- + p \rightarrow e^+ + n \qquad (1)$$

are considered and an upper limit on the intensity of this component of the cosmic radiation is established.[7]

APPARATUS

The detection system is shown schematically in Fig. 1. As an extensive discussion of the details of the design and construction of the system has already been published[5] only a brief summary will be given here.

TABLE I. Lower half-life limits.

Assumed decay mode	Lifetime limit in units of 10^{28} years
$p^+ \rightarrow \pi^+ + \nu$	3
$p^+ \rightarrow \kappa^+ + \nu$	1
$p^+ \rightarrow e^+ + \gamma$	0.6
$p^+ \rightarrow \mu^+ + \gamma$	4
$n \rightarrow \pi^+ + e^-$	4
$n \rightarrow \mu^+ + \kappa^-$	3

* Supported in part by the U. S. Atomic Energy Commission.
† This paper is based on a thesis submitted in partial fulfillment of the requirements for the degree of Doctor of Philosophy at Case Institute of Technology.

[1] E. C. G. Stückelberg, Helv. Phys. Acta **11**, 225, 299 (1938).
[2] E. P. Wigner, Proc. Am. Phil. Soc. **93**, 521 (1949); Proc. Natl. Acad. Sci. U. S. **38**, 449 (1952).
[3] F. Reines, C. L. Cowan, Jr. and H. W. Kruse, Phys. Rev. **109**, 609 (1957).
[4] G. K. Backenstoss, H. Frauenfelder, B. D. Hyams, L. J. Koester, Jr., and P. C. Marin, Nuovo Cimento **16**, 749 (1960).
[5] C. C. Giamati and F. Reines, Phys. Rev. **126**, 2178 (1962).
[6] In a recent experiment by M. G. K. Menon, P. V. Ramana Murthy, B. V. Sreekantan, and S. Miyake, a detector was operated at a depth of 9200 feet in the Kolar Gold Fields, Mysore State, South India. No particles capable of penetrating 5 cm of lead were observed. As was pointed out to these investigators by one of us (F.R.) this result can be used to establish a limit on the stability of nucleons against decay into muons and pions. For the case of a proton decaying into a muon, they have calculated a lifetime limit of 3×10^{28} years. The limit for decay into pions would be similar. Owing to the presence of the lead, the system was much less sensitive to decay modes involving K mesons, electrons and gamma rays. (Private communication from Miyake to Reines.)
[7] The data have also been interpreted in terms of the elastic scattering of solar neutrinos by electrons in the inner detector. An upper limit has been established on the cross section flux product for the elastic scattering process. This product is within a factor of ~20 of theoretical expectations. F. Reines and W. R. Kropp, Phys. Rev. Letters **12**, 457 (1964).

A. Inner Detector

The inner detector (B) was a stainless-steel cylinder, 60.5 cm in diameter and 72 cm high, filled to a depth of 69 cm with approximately 200 liters of Decalin based scintillator. The fluid was viewed by four DuMont-6364 photomultiplier tubes which were grouped into two banks (I and II). The high voltage for each bank was obtained from a separate power supply to minimize false coincidences.

(*1*) *Calibration.* The energy scale of the inner detector (B) and its associated electronics was established from the cosmic-ray spectrum shown in Fig. 2. This spectrum represents the pulse-height distribution obtained underground from cosmic rays passing through B during an 878-h period of the experiment. In compiling this curve one roll was selected as the standard to which all other data were normalized. Observed in the spectrum is the "through peak" resulting from the passage of minimum ionizing particles through B. The peak at 116 MeV corresponds to the amount of energy deposited in B by a minimum ionizing particle passing along the most probable path. It is calculated from the average depth of the liquid assuming an energy deposition of 1.6 MeV per cm, adding a 5% correction for fluctuations in energy loss and the angular distribution of the cosmic rays. The measured peak location was matched with a pulser, so determining the energy calibration for the detector.

(*2*) *Stability.* The gain of the B detector and its associated electronics was checked periodically by means of a Y^{88} source. The source was placed under the detector and the peak due to the 1.9-MeV gamma was located with a 400-channel pulse-height analyzer, and then related to a pulser. A typical gamma calibration spectrum is shown in Fig. 3. Changes occurred in the equipment due to aging and temperature variations. However, calibrations were made often enough to enable determination of the gains to within a few percent. The pulser was found, by referral to a dc voltmeter, to be constant to $\pm 1.2\%$. As an additional check, the pulser was occasionally matched against a second identical pulser with which it agreed to within 2%.

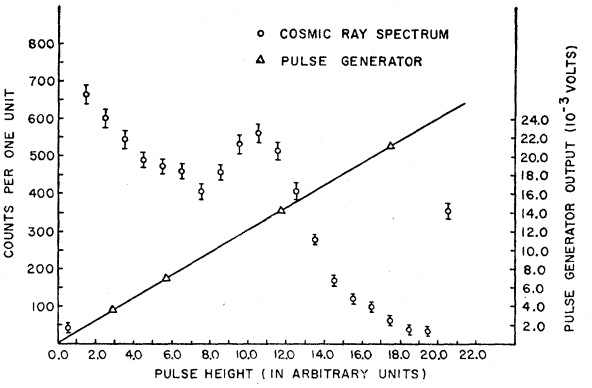

FIG. 2. Pulse-height spectrum produced by cosmic rays in the inner detector as measured underground in 878 h.

B. Anticoincidence Detector

The Čerenkov anticoincidence detector (A) was a sheet-iron cylinder approximately 2.4 m in diameter and 2 m high. An insert of the same material was bolted and sealed to a hole in the base plate of the detector, and served to house the B detector and its iron shield. The detector was painted white and filled to a depth of 184 cm with approximately 7200 liters of distilled water in which was dissolved a wavelength shifter (35 g of β methyl umbelliferone).[8] The water was viewed by 46 balanced and ganged 5-in. DuMont-6364 photomultiplier tubes.

This detector was operated at the highest sensitivity consistent with an acceptable noise level as dictated by the consequent deadtime of the system. No absolute energy calibration was made.

C. Shield

The shield consisted of 7.5 metric tons of steel (99.4% Fe) in the form of three inch square billets

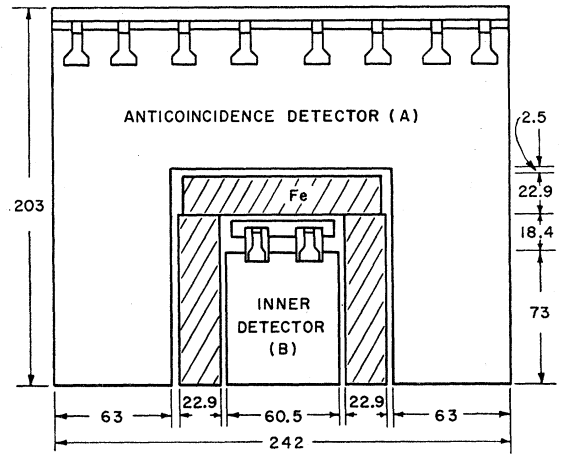

FIG. 1. Schematic diagram of the detector system.

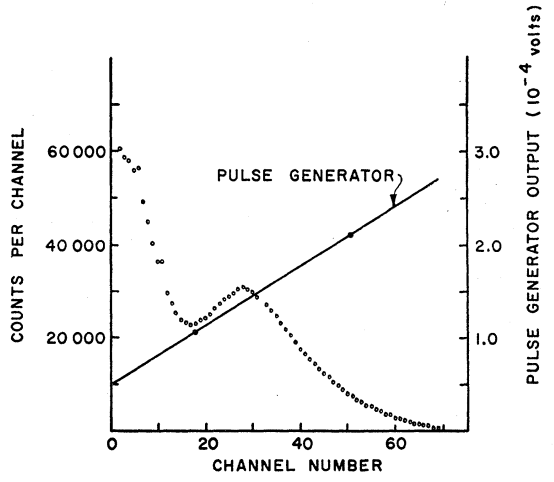

FIG. 3. Y^{88} calibration spectrum.

[8] N. A. Porter, Nuovo Cimento 5, 526 (1957).

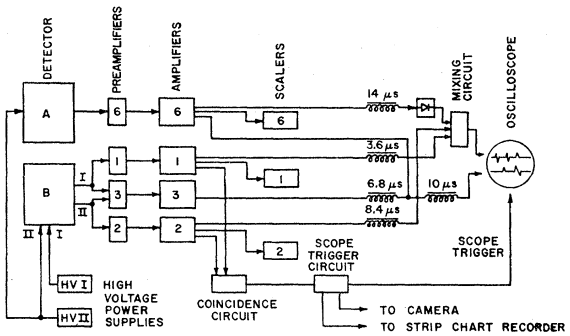

FIG. 4. Block diagram of the detectors and associated electronics.

placed in the space between the two detectors. The minimum shield thickness was approximately 23 cm.

D. Electronics

A block diagram of the detectors and the electronics instrumentation is shown in its final form in Fig. 4. During the course of the experiment changes were made to increase the amount of information presented to the recording oscilloscope. The additional data served to increase the effectiveness of the anticoincidence guard and allowed for certain self-consistency checks.

To illustrate the operation of the system we trace the sequence of events initiated by a cosmic ray passing through both detectors. A portion of the energy deposited by the cosmic ray produces pulses at the input of each of the four preamplifiers. If the energy deposition in B is sufficiently great to trigger output pulses from the integral discriminators of amplifiers 1 and 2, a coincidence is recorded, and a signal sent to a master trigger circuit. This circuit starts the oscilloscope sweep, actuates the camera and notes the event on a strip chart recorder. While the coincidence information is being digested the signals to be photographed are stored in delay lines for proper time presentation on the dual-beam oscilloscope.

On the lower beam, after a base line trace of 10 μsec, the triggered output of the integral discriminator of amplifier 6 records the passage of the cosmic ray through detector A. This is followed 5.8 μsec later by the output pulse of amplifier 3 which is proportional to the sum of the outputs of banks I and II of B, and therefore measures the total energy deposited by the cosmic ray. Thus the presence of these two pulses in the proper time sequence indicates the passage of a cosmic ray through the system. The absence of the first pulse indicates the absence of a charged particle either penetrating or produced in the anticoincidence detector and would be characteristic of a neutrino or a nucleon decay event. Possible sources of background signals are discussed below.

The upper beam displayed the amplified outputs of amplifiers 1, 2, and 6, and served primarily to check the operation of the system. The presence of the 1 and 2 pulses showed that the coincidence unit and the integral gates of these amplifiers were functioning properly. The presence of the amplified output pulse from amplifier 6 showed that its integral gate was functioning and in addition allowed for detection of cosmic rays which deposit insufficient energy in A to trip the gate. The absence of the detector A pulse (amplifier 6) would again be characteristic of a neutrino or nucleon decay event.

Environmental conditions necessary for long-term stability of the electronics were provided by an air-conditioned structure.

EXPERIMENTAL RESULTS

The system was operated for a total of 4500 h. During this period 22 events were observed in the B detector, unaccompanied by anticoincidence pulses. The spectrum of these events is shown in Fig. 5.

Figure 6 shows typical waveforms observed on the oscilloscope during the course of the experiment: (a)–(c) and (d)–(f) show the evolution of the mode of data presentation, the first group of three being characteristic of a cosmic ray passing through both detectors, and the second group of three, of a neutrino or nucleon decay event. (g) and (h) result from muon decay and (i)–(j) are typical noise bursts.

The observed noise bursts often occurred in groups of three or more, and frequently could be associated with equipment such as the air conditioner, or with mining activities in nearby shafts and tunnels. These noise pulses could be distinguished visually without ambiguity and served only to increase the dead time of the system, an unimportant consequence since the total dead time correction, including these pulses and those due to cosmic rays, is negligible.

From the observed singles rates in the two banks of tubes in the inner detector it is calculated that the total number of accidental coincidences leading to unaccompanied B events is less than 0.2. The number of accidental anticoincidence pulses from detector A can be calculated assuming the observed B-only, event rate. This leads to a correction of less than 0.5 for the duration of the experiment. It is within the accuracy of the experiment to neglect these effects.

POSSIBLE SOURCES OF UNACCOMPANIED INNER DETECTOR EVENTS

A number of natural and instrumental sources have been investigated in an attempt to determine their effectiveness as causes of the observed signal.

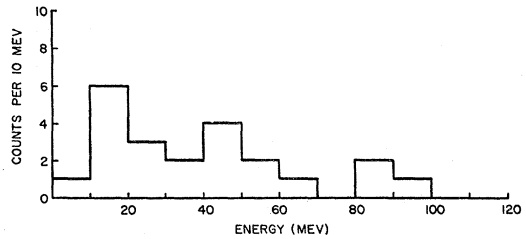

FIG. 5. Pulse-height spectrum of inner detector events which were unaccompanied by anticoincidence pulses.

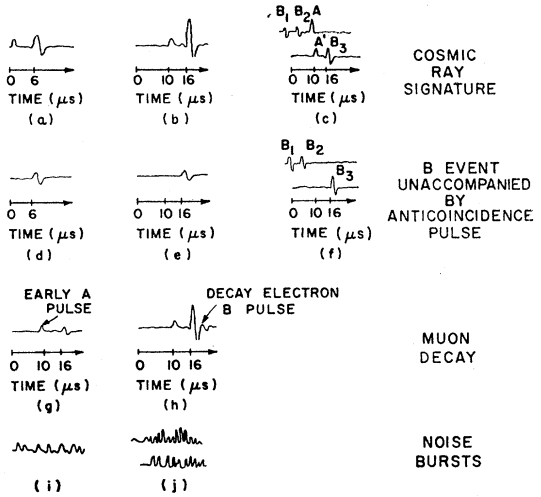

FIG. 6. Tracings of typical waveforms observed during the experiment: (a)–(c), cosmic ray signatures; (d)–(f), B events unaccompanied by anticoincidence (A) pulses; (g), meson decay in the iron shield; (h), meson decay in the scintillator, (i), (j), typical noise bursts. In (c) from left to right, the pulses are: lower beam, the discriminator output of amplifier 6 (A′) and the amplified output of amplifier 3 (B_3); upper beam, the amplified outputs of amplifiers 1 (B_1[3]), 2 (B_2), and 6 (A).

A. Natural Sources

(*1*) *Radioactivity.* The high-energy requirements (8–10 MeV) of the B-detector electronics discriminate against the background due to single radioactive decays. Nevertheless, natural radioactivity can produce acceptably high-energy pulses when several events occur within the resolving time of the circuitry. The "pileup" of two events is estimated from the low-energy background observed with the detector to account for between 0.1 and 0.7 acceptable pulses during the experiment. The spread is due to uncertainty in the energy calibration.

(*2*) *Muon decay.* A muon, decaying several microseconds after stopping in the shield, can send a high-energy electron ($\leq$52 MeV) into the B detector. Since it is the event in B which triggers the electronics, the information provided by the anticoincidence detector, A, is lost unless some provision is made to observe it for several muon lifetimes prior to each event. During the last 3500 h of the experiment such a scan was made by delaying the anticoincidence information presented to the oscilloscope for 10 μsec. With this delay approximately 99% of all events associated with muon decay in the iron are recognizable. The early A pulse in Fig. 6(g) is characteristic of a delayed decay event.

An estimate of the expected signal from muon decay follows. From the slope of the intensity-depth curve for the cosmic-ray intensity underground[9] the number of muons which stop in the iron within the decay electron range of the B detector was determined. Since negative muons are practically all absorbed by the iron nuclei, only the positive fraction, or about half, of the stopped muons can be expected to decay. This leads to an estimated rate of <4 events in 4500 h, a value which is consistent with observations made in the last 3500 h of the experiment. Thus it seems reasonable that perhaps one or two of the events observed during the first thousand hours were due to muon decay.

Muons which stop in the B detector and then decay have the typical cosmic-ray signature in addition to a second B detector pulse [Fig. 6(h)]. Hence such events were always recognized and rejected.

(*3*) *Charged cosmic rays which escape detection in the anticoincidence detector.* The anticoincidence factor is defined as the ratio of the number of events observed in B which were unaccompanied by events in A, to the number of events which were observed in both A and B simultaneously. Table II gives the anticoincidence factors observed during various periods of the experiment and the corresponding gains of the anticoincidence electronics. Owing to changes in the B gate energies, exact comparison is not possible, but the numbers indicate an increased anticoincidence efficiency with increased electronic gain. It is therefore likely that at least some of the observed B events were due to less than perfect anticoincidence efficiency. Conceivably, events occurring in the regions of the A detector most remote from the photomultiplier tubes were not observed with 100% efficiency.

(*4*) *Neutral particles.* Two neutral radiations, neutrons and photons, are of interest as possible sources of background. Both have finite probabilities of passing through A without interacting and then interacting in B. The reduction in the flux of these radiations underground is a prime reason for the location of the experiment.

Neutrons: High-energy neutrons (>10 MeV) observed at these depths result from muon induced stars. The flux of such neutrons leaving the walls, floor, and ceiling of the tunnel can be estimated from the muon flux,[9] the cross section for star production by muons,[10] and the neutron interaction cross section in the salt.[11] From the solid angles subtended by B at various regions

TABLE II. Anticoincidence factors.

Time average lower gate energy of detector B (MeV)	Relative gain of detector A electronics	Anticoincidence factor (10^{-4})	[Anticoincidence factor]$^{-1}$ (10^3)
8±2	1	8±3	1.2±0.4
9±2	2	6±3	1.6±0.7
9±2	>2	4±1	2.2±0.7
9±2[a]	···	6±1[a]	1.7±0.4[a]

[a] Gate energies and anticoincidence factors averaged for entire experiment.

[9] P. H. Barrett, M. Bollinger, G. Cocconi, Y. Eisenberg, and K. Greisen, Rev. Mod. Phys. 24, 133 (1952).

[10] B. Peters, in *Handbook of Physics*, edited by E. U. Condon and H. Odishaw (McGraw-Hill Book Company, Inc., New York, 1958), Chap. 12, pp. 9-233.

[11] Evans, *The Atomic Nucleus* (McGraw-Hill Book Company, Inc., New York, 1955), Chap. 14, p. 457.

of the tunnel and from the efficiency with which a neutron can penetrate A and the shield without an interaction and then interact in B, the expected background can be determined. In this way the neutron background is estimated to be <0.1 for the duration of the experiment.

Gamma Rays: Gamma rays observed at these depths are produced as bremsstrahlung quanta by muons and by electrons which are secondary to the muon and photon flux. This complex mechanism of production and the wide range of interesting energies make simple estimates of the gamma intensity and energy spectrum impossible. We consider here the various aspects of gamma-ray production and interaction and reach some qualitative conclusions as to the likelihood of background produced by gamma rays.

A gamma ray which is effective in producing a background event in B must be unaccompanied by charged particles which enter the anticoincidence detector. Hence, to prevent shower formation the gamma ray must be produced, on the average, within a radiation length of the detectors. The efficiency with which such a gamma ray can produce a background event in B is energy-dependent, rising from a value of $\sim 10^{-4}$ at 50 MeV to ~ 0.2 at $\geq 10^4$ MeV. These facts, together with the characteristically sharply forward peaking of the bremsstrahlung radiation and the long radiation length of the muon ($\sim 4\times 10^4$ times the gamma-radiation length) virtually eliminate background due to gammas from muon bremsstrahlung.

High-energy gamma rays ($>5\times 10^4$ MeV) can also be eliminated as likely sources. The presence of the Fe shielding (~ 13 radiation lengths) insures shower production by such photons. On leaving the Fe, showers in this energy range contain many electrons with a total energy[12] of $>10^3$ MeV and would thus deposit large energies in B. Since no events were observed with $E>100$ MeV, such gammas appear to be unimportant as a source of background.

This leaves electron-produced gamma rays with energies $<5\times 10^4$ MeV. In view of the previous arguments, viz., the tendency of photons to make showers, the close angular association of the parent and secondary, and the reduced detection efficiency at low energies, it seems improbable that these gammas are a source of background.

Despite the above arguments, the rarity of the observed events and the extended duration of the experiment, make it necessary to conclude that "improbable" is not a sufficiently strong condition and that the question of gamma rays as a source of background is still open.[13]

[12] B. Rossi and K. Greisen, Rev. Mod. Phys. **13**, 240 (1941).

[13] In future experiments this source of background could be greatly decreased by the use of a sufficient thickness (several radiation lengths) of a high-Z material in close proximity to the anticoincidence detector. This would insure shower production by incident gammas prior to entering the anticoincidence detector. The shielding must be sufficiently close to the detecting medium to prevent electrons from radiating and then scattering so as not to enter the detector.

(5) *Scattered low-energy cosmic rays.* Low-energy muons, electrons, and gamma rays scattered through large angles could contribute background events by entering the B detector from below and stopping in the shield, thus avoiding the A detector. The magnitude of this effect can be estimated by comparison with a recent experiment on the effectiveness of anticoincidence guards.[14] Using a detector system similar, except in size, to that employed in the present experiment, an unaccompanied inner detector event rate of 7.7 h^{-1} was observed under 650 g/cm^2 of iron. Assigning all of these events to scattered radiation, and scaling the results to the mine depth by the reduction in the vertical intensity of the cosmic radiation gives ~ 2 events in 4500 h. Since the system used in the present experiment has an inner detector with base area smaller by a factor of 0.9 and an anticoincidence guard with radius larger by a factor of 1.4, and since the muon spectrum is hardened with depth, the result, two events in 4500 h, should be a valid upper limit on the number of events which can be attributed to scattering.

B. Instrumental Sources

(1) *Coincidence circuit.* An intermittent failure of the coincidence circuit could result in its response to a noise pulse from one of the two banks of tubes of the B detector. This would lead to a B-only signal. This possibility was checked during the last 500 h of the experiment by displaying on the oscilloscope, the individual pulses from each bank [pulses B_1 and B_2 of Fig. 6(c)]. All signals, including three unaccompanied B events, observed during this period indicated proper operation of these systems.

(2) *Anticoincidence detector integral discriminator.* Since the signature of an event in A was the triggered output pulse from this circuit, an intermittent failure could result in a B-only signal. To check the operation of this portion of the electronics, the last 500 h of data was taken with the amplified output pulse from the anticoincidence amplifier displayed as the third pulse on the upper beam of the oscilloscope [pulse A of Fig. 6(c)]. The presence of the amplified output pulse also allowed for the possibility of observing events which deposit insufficient energy in A to trigger the discriminator. Three B-only events were observed during this period. In each of these events the amplified output pulse and the discriminator pulse were both absent indicating correct operation.

C. Summary

Several possible sources of background have been considered but whether there is a residual signal, and to what such a signal is due, are questions to which the present experiment and other available information do not provide an answer.

An improved experiment currently in the construction stage should help resolve these questions.

[14] M. K. Moe, T. L. Jenkins, and F. Reines, Rev. Sci. Instr. **35**, 370 (1964).

TABLE III. Summary of component parts [Eq. (10)] of the calculation leading to detector efficiency $f(E_0)$.

Decay modes	N_{eff} (in units of 10^{28} nucleons) Scint	Fe shield	NaCl	$F_{\text{Fe}}(E_0)$[a]	A_{Fe} $(x>x(E_0))$[a]	F_{NaCl} (E_0)[a]	A_{NaCl} $(x>x(E_0))$[a]	A_{scint} $(x>x(E_0))$[a]
$p\rightarrow\pi+\nu$	5.1	25.7	3.6	0.84	0.40	0.84	0.33	0.11
$p\rightarrow k+\nu$	5.1	2.8	3.5	0.31	0.40	0.30	0.33	0.62
$p\rightarrow e+\gamma$	5.1	4.0	0.76	0.45	0.40	0.52	0.33	0.17
$p\rightarrow\mu+\gamma$	5.4	29.1	4.1	0.83	0.40	0.84	0.33	0.13
$n\rightarrow\pi+e$	4.6	29.5	3.9	0.84	0.40	0.84	0.33	0.17
$n\rightarrow\mu+k$	4.6	20.4	2.7	0.72	0.40	0.73	0.33	0.64

[a] $E_0=87$ MeV.

NUCLEON LIFETIME CALCULATION

The lifetime limits which can be calculated with the experimental data (Fig. 5) understandably depend on the assumed nucleon decay modes. Those considered are shown in Table III along with the calculated lower half-life limits which were obtained assuming that nucleons decay only by the individual process in question. These processes are typical, two particle decays which are consistent with the conservation of energy-momentum, spin, and charge, but not with lepton conservation. Lifetime limits for other decay modes can be obtained in similar fashion.

To calculate the half-life limit for each decay mode we must determine: (1) the number of nucleons which can contribute observable decay products and (2) the fraction of the observed events which is consistent with the decay scheme. The half-life $T_{1/2}$ can then be calculated for each mode from the time-honored formula

$$T_{1/2}=N\ln 2/(\Delta N/\Delta T), \qquad (2)$$

where N is the effective number of nucleons and $\Delta N/\Delta T$ is the decay rate.

A. Effective Number of Nucleons

An exact calculation of the effective number of nucleons in the B detector and its environment depends on the ranges of the decay products, and on the detector and shield geometries. In view of the meager statistics associated with the experimental data and the absence of any clearly identifiable cause of the signal we expedite the calculation by making a number of simplifying assumptions, each one conservative. Here the conservative view underestimates the effective number of nucleons and hence the nucleon lifetime.

It is convenient to divide the nucleons into three classes: free protons, bound protons, and bound neutrons. The free protons are the hydrogen nuclei of the scintillator which are chemically bound by only a few electron volts to the Decalin carbon rings. The bound nucleons are the protons and neutrons of the iron shielding, the salt beneath the detector and the scintillator carbon.

(*1*) *Free protons.* Since there is a minimum-energy deposition, and hence path length, in the scintillator required for detection, a charged particle resulting from a free-proton decay near a detector wall would be seen with $<100\%$ efficiency. Accordingly, the actual number of free protons in the scintillator must be reduced by a small fraction to compensate for these undetectable decays. While this minimum path depends on the decay particle and on its energy, the smallest possible effective number of protons is obtained if the particles are assumed to be minimum ionizing. Thus we use the minimum ionization path length of 6.2 cm corresponding to a 10-MeV energy deposition in the scintillator. In Sec. B, the distribution of path lengths which start anywhere in the cylinder and end on its surface is considered and the fractional number of path lengths greater than any given length is calculated. The results of the calculation are given in Fig. 7 where x is the path length divided by the cylinder diameter (60.5 cm). From this spectrum it is seen that 84% of such paths are longer than 6.2 cm. Hence the decay of 84% of the free protons in the detector would be detected with 100% efficiency. The other 16% would be seen with an efficiency varying from 0 to 100%. The total number of free protons is given by

$$N=\pi b^2 h\rho,$$

where ρ is the free proton density. ($\rho=6.96\times10^{22}$ protons/cm^3.) Thus the total number of free protons is 1.38×10^{28} and the effective number is 1.2×10^{28}.

(*2*) *Bound nucleons.* The number of bound nucleons associated with the scintillator can be obtained by multiplying the free-proton result by the ratio of the number of bound neutrons (or protons) to the number of free protons in a Decalin molecule. This ratio is 10/3. For bound protons a correction identical to that made in the free-proton case is necessary so that the effective number of bound protons in the detector is 4.0×10^{28}. For neutrons, two charged particles are produced in each decay mode considered and since at

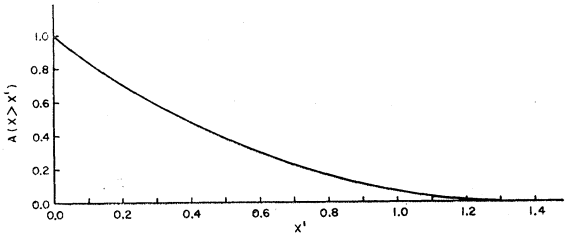

FIG. 7. Fraction of path lengths A $(x>x')$, greater x', for paths which start anywhere in the cylinder and end on its surface.

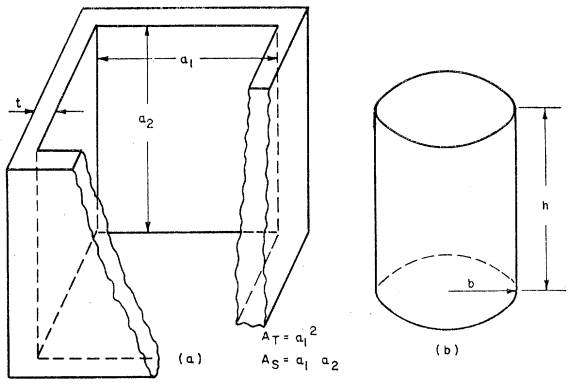

FIG. 8. Geometry of the iron shield (top slab removed) and the inner detector showing the geometric parameters used.

least one particle always heads into the scintillator no correction need be made for events occurring near the detector walls. The number of bound neutrons in the scintillator is therefore 4.6×10^{28}.

The effective number of nucleons in the environment of the B detector is calculated in two steps. First, we determine the number of nucleons which can, if they decay, give products capable of penetrating to the cavity in which the detector is located. The second step consists of determining the fraction of these decay products which would be seen by the detector. Consider the iron shield: It is conveniently divided into four side slabs and a top slab. In Appendix I the number of nucleons per unit area of semi-infinite slab which, if they decay, could produce detectable products is calculated.

The semi-infinite slab results [Eqs. (I2a) and (I2b)] should reasonably approximate the relevant number of nucleons in each slab provided the area A in these equations is taken in each case to be the slab area visible to the detector and t is taken as the slab thickness.

The salt beneath the detector can be similarly treated except that the relevant number of nucleons is limited by the range of the decay products.

Having established the number of nucleons which could in the event of nucleon decay give particles emerging from the slabs, we now determine the fraction of these which would actually be detected. For particles originating in a side slab a reasonable estimate of this fraction f_S is the ratio of the cross-sectional area of the cylinder $2bh$ (Fig. 8) to the cross-sectional area A_s of the shield interior. For particles originating in the top or bottom slabs, the fraction f_T can be taken as the ratio of the circular cross-sectional area of the detector, πb^2, to the area A_T of the slab visible to the detector.

Thus for the iron shield, N_{eff}, the effective number of nucleons, is given by

$$\begin{aligned} N_{\text{eff}} &= (4f_S A_S + f_T A_T)\times\tfrac{1}{4}\rho_{\text{Fe}} R_{\text{Fe}} \qquad (R_{\text{Fe}} \le t) \\ &= (4f_S A_S + f_T A_T)\times\tfrac{1}{2}\rho_{\text{Fe}} t(1-t/2R_{\text{Fe}}), \quad (R_{\text{Fe}} \ge t) \end{aligned} \tag{3a}$$

while for the NaCl

$$N_{\text{eff}} = f_T A_T \times \tfrac{1}{4}\rho_{\text{NaCl}} R_{\text{NaCl}}. \tag{3b}$$

In each material ρ is the nucleon density and R is the range of the decay product.

B. Events Attributable to Nucleon Decay

Since, as we now show, the energy distribution of the observed events (Fig. 5) differs from that expected from the nucleon decay modes considered, only a portion of these events should be attributed to such processes. As remarked earlier, a detailed calculation of the expected decay spectrum would be more difficult than is warranted by the small number of events observed. Consequently, a simpler estimate of the decay rate is made, guided by the criterion that it should err on the side yielding a lower limit for the lifetime. First, the relative weight of the decay spectrum above and below a given energy E_0 is estimated. The maximum number of events consistent with nucleon decay is then determined by assuming that *all* observed events with energies greater than E_0 are associated with nucleon decay. The value of E_0 is chosen is that which minimizes the total number of acceptable events. Since a conservative estimate of the decay rate is required, any assumption made in the relative weight calculation must overestimate the weight of the spectrum below E_0. The calculation is done in two parts, considering in turn decay products originating outside and inside the detector.

(*1*) *Expected energy distribution from decay products produced outside the detector.* If r is the distance a decay product must travel in the slab to have its kinetic energy reduced to E_0, it follows from Appendix I that the fraction of the decay products which leaves the slab with kinetic energy $>E_0$ is given by

$$F(E_0) = \int_0^{r,t} f(r,z)dz \Big/ \int_0^{R,t} f(R,z)dz, \tag{4}$$

where the upper limit in each integral is the smaller of the two distances given, and

$$\begin{aligned} F(E_0) &= R(2r-t)/r(2R-t) \qquad R>t, r>t \\ &= Rr/t(2R-t) \qquad R>t, r<t \\ &= r/R \qquad R<t, r<t. \end{aligned} \tag{5}$$

The use of the infinite slab formulas is reasonable here since the errors introduced by edge effects into both numerator and denominator are small.

The fraction of the decay particles which leave the slabs with kinetic energies $>E_0$, but which deposit $<E_0$ in the detector must now be determined. It will be assumed for simplicity that all decay particles with kinetic energy in excess of E_0 are minimum ionizing and that the particle paths are straight lines. These assumptions are conservative since for a given straight-line path the minimum energy deposition associated with these energies gives the maximum weight possible to the spectrum below E_0. The problem is therefore reduced to one of estimating the distribution of path lengths through a cylinder with angular weighting

TABLE IV. Component spectra and environmental regions.

Spectrum \ Region	Top slab	Bottom slab	Side slab	Ring
Top-base	Isotropic cyl. spectrum conservative	···	···	Isotropic cyl. spectrum conservative
Top-wall	Isotropic cyl. spectrum conservative	···	···	Isotropic cyl. spectrum nonconservative
Wall-top	···	Negligible	Isotropic cyl. spectrum conservative	···
Wall-wall	···	Negligible	Isotropic circle spectrum conservative	Negligible
Wall-base	Negligible	···	Isotropic cyl. spectrum conservative	Negligible
Base-top	···	Isotropic cyl. spectrum conservative	···	···
Base-wall	···	Isotropic cyl. spectrum conservative	···	···

appropriate to the slab sources. The main feature of the angular distribution of particles which originate in a slab and enter the detector cavity is a relatively larger number with small angles to the slab normal than in the isotropic case.

It is convenient at this point to divide the spectrum into component spectra as shown in Table IV, where for example, the notation "top-base" refers to the spectrum of lines which start on the cylinder top and end on its base. It is also convenient to divide the material surrounding the cylinder into various regions as shown in Fig. 9 and listed in Table IV.

Consider first the spectra produced by particles originating in either the top or bottom slabs. Because of symmetry, these spectra will be identical, and hence we need discuss only the top slab. Since all top-base lines are longer than those associated with E_0 and since the forward peaking serves only to increase the weight, i.e., fraction of paths in the top-base category, the isotropic top-base spectrum with isotropic weighting can be used. This spectrum has been calculated[15] and

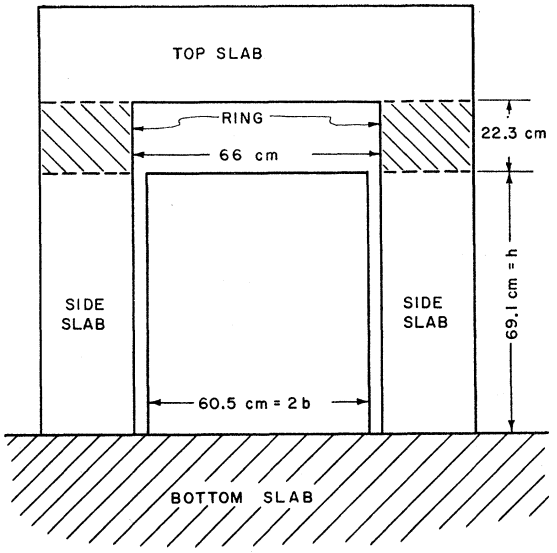

FIG. 9. Regional division of the environment of the inner detector.

[15] R. J. Wagner, Rev. Sci. Instr. 31, 271 (1960).

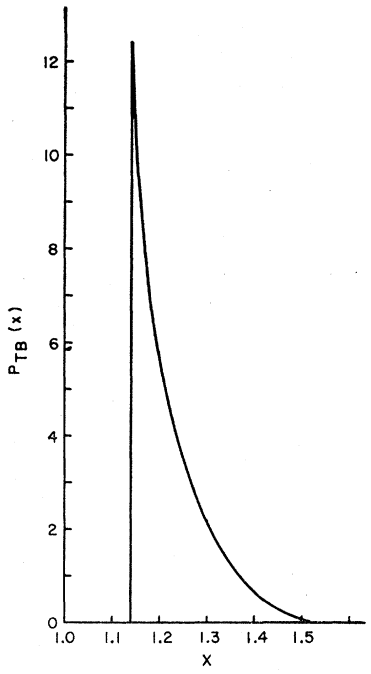

FIG. 10. Isotropic top-base spectrum, $P_{TB}(x)$

is shown in Fig. 10. Similarly, the isotropic top-wall spectrum with isotropic weighting can be conservatively employed since the forward peaking leads to increased path lengths and reduced weighting. This spectrum is shown in Fig. 11.[15]

Consider next the spectra of particles originating in the side slabs. We observe that the previous comments regarding the top-wall spectrum also apply to the wall-top and wall-base spectra. However, it has not been shown that the isotropic spectrum conservatively approximates the wall-wall spectrum; hence a different approximation will be employed in this case. A derivation of the wall-wall spectrum could be couched in terms of two angular variables θ and ϕ (Fig. 12). Moving along the x axes over the length of the slab, the planes defined by the equation ϕ=constant, intersect the cylinder in rectangles. For each of these rectangles, the path-length distribution can be calculated with the

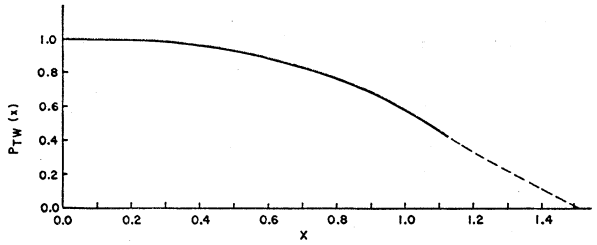

FIG. 11. Isotropic top-wall spectrum, $P_{TW}(x)$. The dashed portion of the curve is extrapolated.

proper angular weighting, and the results summed over the rectangles. Summing this result over all ϕ, again with proper weighting for the angular distribution, yields the desired path-length distribution. However, since we wish a conservative estimate to the actual spectrum, the calculation can be simplified by assuming that all particles leave the slab with $\theta=\frac{1}{2}\pi$. This gives the entire weight of each rectangle to the shortest possible wall-wall path within the rectangle, so reducing the problem to the two-dimensional one shown in Fig. 13. For a given ϕ, the spectrum associated with each slab is now that due to a portion of a circle in a unidirectional flux. Because of symmetry, the full circle and semicircle have identical path-length distributions. This fact together with the relative forward peaking of the slab spectrum suffices to show that the full circle distribution gives a conservative approximation to the spectrum associated with any ϕ. Thus in Fig. 13 for $\phi\leq 45°$, the circle spectrum can be used for the particles from slab 1. Over this same region in ϕ, particles from slab 2 fill in that portion of the full circle not used by those from slab 1. In view of the forward peaking of the angular distribution, slab 2 particles have less weight than those from slab 1. Hence the full circle spectrum can be used for both slabs taken together. When ϕ is greater than 45°, the same argument can be made with the roles of the slabs interchanged. Thus the circle spectrum is valid for any ϕ and so is a conservative approximation to the entire wall-wall spectrum. This distribution is easily computed to be

$$P(x)dx=[x(1-x^2)^{-1/2}]dx, \tag{6}$$

where $x=L/2b$, L is the path length, and b is the cylinder radius. The spectrum is shown in Fig. 14.

The various spectra must now be superposed with the appropriate weighting. Relative to the isotropic

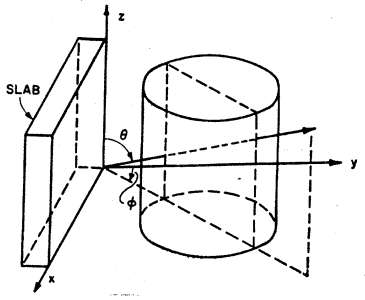

FIG. 12. Slab and detector geometry for calculating $P_{WW}(x)$.

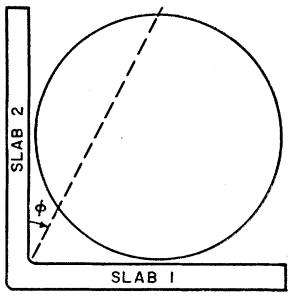

FIG. 13. Simplified geometry for calculating a conservative approximation to $P_{WW}(x)$.

distribution, the expected angular distribution reduces the weight associated with the wall-top and wall-base spectra while increasing the weight associated with the wall-wall spectrum. Since both the wall-top and wall-base spectra emphasize path lengths shorter than the E_0 path length more heavily than does the wall-wall distribution, use of the isotropic weighting for each component spectrum is conservative.

A consideration of the spectrum exhibited by decay products originating in the "ring" region of the shield completes the analysis. The effect of the forward peaking here is to reduce the average path length for the top-wall traversals as compared with the isotropic case. Hence the isotropic spectrum cannot be used. The volume of the ring is approximately 20% of the total shield volume and therefore, because of its location, can contribute at most 10% of the observed decay events which originate in the iron. It will be conservatively assumed that all of these deposit less than E_0 in the detector.

For the 0.9 $F_{Fe}(E_0)$ decay products produced in the iron, a composite of the spectra shown in Figs. 10, 11, and 14 can be employed, the weighting being that for an isotropic flux incident on the detector. These weightings are[15]

$$N_{TB}=\tfrac{1}{4}\pi^2[(4b^2+h^2)^{1/2}-h]^2J, \tag{7a}$$

$$N_{WT}=\pi^2b^2J-N_{TB}, \tag{7b}$$

and

$$N_{WW}=2\pi^2bhJ-2N_{WT}, \tag{7c}$$

where J is the number of incident particles per unit area per unit solid angle, b and h are the cylinder parameters defined in Fig. 8(b), and, for example, the notation N_{TB} refers to the number of lines starting at the cylinder top and ending at its base. The conservatively expected spectrum is given by

$$P_{Fe}(x)=\frac{P_{WW}(x)N_{WW}+3P_{WT}(x)N_{WT}+P_{TB}(x)N_{TB}}{N_{WW}+3N_{WT}+N_{TB}} \tag{8a}$$

and is shown in Fig. 15. For the $F_{NaCl}(E_0)$ decay products produced in the NaCl, the expected spectrum is given by

$$P_{NaCl}(x)=\frac{P_{WT}(x)N_{WT}+P_{TB}(x)N_{TB}}{N_{WT}+N_{TB}}, \tag{8b}$$

and is shown in Fig. 16.

(2) *Expected energy distribution from decay products produced inside the B detector.* As the decay products are assumed to be minimum ionizing, the energy spectrum which would be exhibited by particles created in the detector is determined by geometrical considerations only. The appropriate path-length distribution is that for paths which start anywhere in the cylinder and end on its surfaces. This distribution gives the fraction of the particles which would deposit an energy $>E_0$ in the detector. Since the spectrum of lines which start on the top of a cylinder and end on its sides or base is known for a cylinder of any specific depth, the desired distribution from the entire cylindrical detector can be calculated. Let $A_y(x>x')$ be the fractional weight associated with path lengths greater than $x'[=x(E_0)]$ for paths which start on the top of a cylinder of depth y and end on its surface. Then, the fractional weight $A(x>x')$ assigned to path lengths greater than x' for paths starting anywhere in a cylinder of depth h is given by

$$A(x>x')=\sum_{y=0}^{y=h} A_y(x>x')/\sum_{y=0}^{y=h} A_y(x>x=0), \quad (9)$$

where the summation is taken over the total depth, h, of the cylinder. The component spectra used to find the values of $A_y(x>x')$ are shown in Fig. 17. The resultant fractional area $A(x>x')$ is shown in Fig. 7.

Summing up the preceding arguments, the fraction of events $f(E_0)$ which deposit energy in excess of E_0 in the cylinder is given by

$$\begin{aligned} f(E_0)=\{&0.9F_{\mathrm{Fe}}(E_0)A_{\mathrm{Fe}}[x>x(E_0)](N_{\mathrm{eff}})_{\mathrm{Fe}} \\ &+F_{\mathrm{NaCl}}(E_0)A_{\mathrm{NaCl}}[x>x(E_0)](N_{\mathrm{eff}})_{\mathrm{NaCl}} \\ &+A_{\mathrm{scint}}[x>x(E_0)](N_{\mathrm{eff}})_{\mathrm{scint}}\} \\ &\times\{(N_{\mathrm{eff}})_{\mathrm{Fe}}+(N_{\mathrm{eff}})_{\mathrm{NaCl}}+(N_{\mathrm{eff}})_{\mathrm{scint}}\}^{-1}, \end{aligned} \quad (10)$$

where, for each substance, $A[x>x(E_0)]$ is the fractional weight given to paths longer than $x(E_0)$. The maximum number of events ΔN consistent with any given mode is, finally,

$$\Delta N=N(E>E_0)/f(E_0), \quad (11)$$

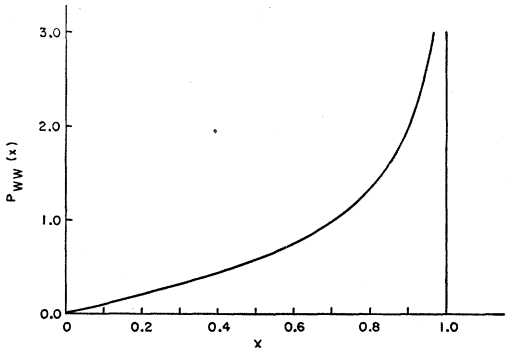

FIG. 14. Circle spectrum approximation to $P_{WW}(x)$. The spectrum goes to infinity at $x=1.0$.

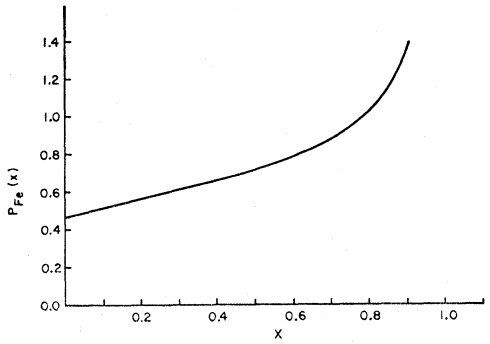

FIG. 15. Portion of the approximation to the spectrum exhibited by decay products which leave the iron slabs with energy in excess of E_0.

where $N(E>E_0)$ is the number of events observed with energy $>E_0$.

Table III summarizes the numerical values for N_{eff}, A, and F.

COSMIC-RAY NEUTRINO LIMITS

The data collected in this experiment can also be interpreted in terms of limits on the neutrino component of the cosmic radiation. The results depend on assumptions made about the interactions and fluxes. Typical of the reactions we assume here are

$$\nu_e+{}_{26}\mathrm{Fe}^{56}\rightarrow {}_{27}\mathrm{Co}^{56}+e^-$$

and

$$\bar{\nu}_e+{}_{26}\mathrm{Fe}^{56}\rightarrow {}_{25}\mathrm{Mm}^{56}+e^+.$$

Although the cross sections can be calculated explicitly as a function of neutrino energy we do not make use of this fact here because the incident neutrino spectrum is not known. Such an interpretation will be made for ν_e, $\bar{\nu}_e$ with energies $\leq$400 MeV. We do not give the corresponding quantities for ν_μ, $\bar{\nu}_\mu$, and for more energetic ν_e, $\bar{\nu}_e$ as other experimental data are available[16] which can be interpreted to give more stringent limits for these neutrinos.

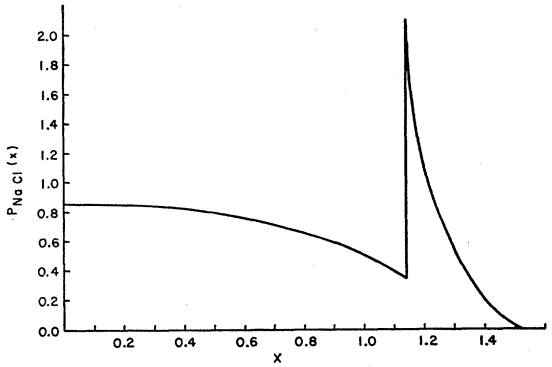

FIG. 16. Approximation to the spectrum exhibited by decay products which leave the salt beneath the inner detector with energy in excess of E_0.

[16] P. V. Ramana Murthy, Ph.D. thesis, University of Bombay, 1962 (unpublished).

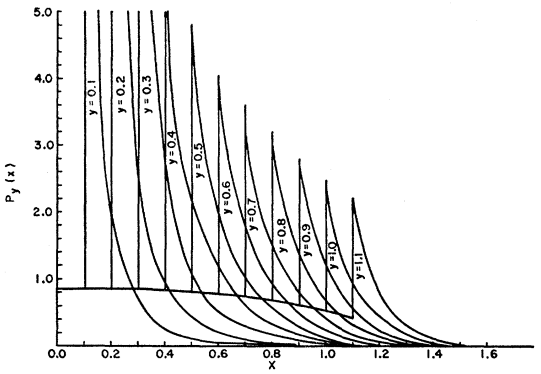

FIG. 17. Component spectra, $P_y(x)$, used to find $A_y(x>x')$. The peaks for $y=0.1$, 0.2, and 0.3 are at $x=21$, 11, and 7.6, respectively.

The limits can be stated in various ways. We first calculate an upper limit on the energy average of the flux cross-section product. For an isotropic neutrino flux, $J_\nu(E_\nu)dE_\nu$, the number of neutrinos at energy E_ν in dE_ν, which cross a unit area of the target material per unit time from all directions is $2\pi J_\nu(E_\nu)dE_\nu$. The isotropic assumption is valid for neutrino energies below 1 GeV.[17] Section A(1) and Eqs. (3a) and (3b) of Sec. A(2) of the Nucleon Lifetime Calculation give as a function of electron energy the number of nuclei $N_{\text{eff}}(E_e)$ which, acting as isotropic electron sources, are observed by the detector with 100% efficiency. The quantity N_{eff} which is known in terms of the electron energy can also be stated in terms of the neutrino energy by making use of the conservation laws. We neglect in this transformation the small variation in electron energy associated with a given neutrino energy. Hence the signal rate $S(=22$ events in 4500 h) is

$$\int_{E_\nu} 2\pi J_\nu(E_\nu)\sigma(E_\nu)N_{\text{eff}}(E_\nu)dE.$$

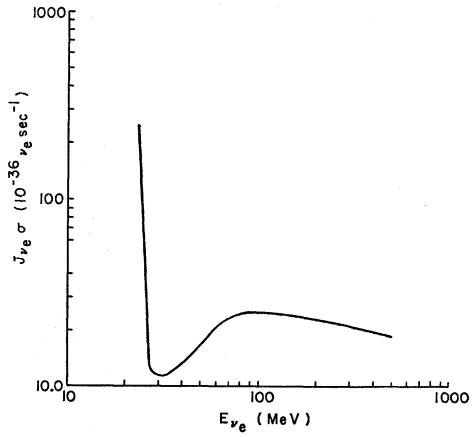

FIG. 18. Upper limit on the product of flux and cross section for neutrinos as a function of neutrino energy.

[17] G. T. Zatsepin and V. A. Kuz'min, Zh. Eksperim. i Teor. Fiz. 41, 1818 (1960) [English transl.: Soviet Phys.—JETP 14, 1294 (1960)].

Replacing $N_{\text{eff}}(E_\nu)v$ by its minimum value $N_{\min}$ over the energy range of interest to obtain an upper limit on $\langle J_\nu\sigma\rangle$,

$$S\geq 2\pi N_{\min}\int_{E_\nu} J_\nu(E_\nu)\sigma(E_\nu)dE_\nu$$

or

$$S\geq 2\pi N_{\min}\langle J_\nu\sigma\rangle[E_{\nu\,\max}-E_{\nu\,\min}].$$

Therefore

$$\langle J_\nu\sigma\rangle\leq\frac{1}{2\pi N_{\min}}\frac{S}{[E_{\nu\,\max}-E_{\nu\,\min}]}.$$

Thus considering the relative number of ν_e and $\bar{\nu}_e$ targets we obtain

$$\langle J_\nu\sigma\rangle\leq 8.5\times 10^{-38}\nu_e \text{ sec}^{-1}$$

and

$$\langle J_\nu\sigma\rangle\leq 3.2\times 10^{-38}\bar{\nu}_e \text{ sec}^{-1};\quad 30 \text{ MeV}\leq E_\nu\leq 400 \text{ MeV}.$$

The large difference is due to the hydrogen in the scintillator.

In a second interpretation we obtain an upper limit on the flux cross-section product as a function of energy. For this purpose it will be conservatively assumed that neutrinos of a given energy are responsible for all observed events consistent with the maximum energy an electron can deposit in the detector.

Here, the signal rate is given by

$$S=2\pi J_\nu\sigma N_{\text{eff}}.$$

Again, N_{eff} is calculated from Secs. A(1) and A(2) [Eqs. (3a) and (3b)] of the Nucleon Lifetime Calculation. The results are shown in Figs. 18 and 19.

ACKNOWLEDGMENTS

Thanks are due to Professor M. F. Crouch and Professor T. L. Jenkins for many valuable discussions, to Dr. C. C. Giamati and A. A. Hruschka for the design and construction of much of the equipment, to R. C. Cassel for his help in collecting data at the mine, and to the Morton Salt Company for their hospitality at the Fairport Harbor Mine.

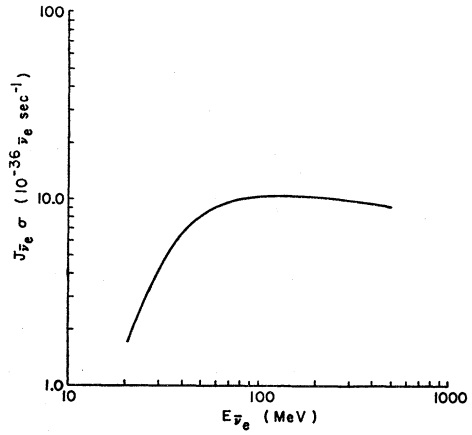

FIG. 19. Upper limit on the product of flux and cross section for antineutrinos as a function of antineutrino energy.

APPENDIX I: EFFECTIVE NUMBER OF NUCLEONS PER UNIT AREA IN A SEMI-INFINITE SLAB

As discussed in Sec. A(2) of the Nucleon Lifetime Calculation, the effective number of nucleons per unit area in each slab of the iron shielding can be approximated by the number per unit area in a semi-infinite slab. Thus consider the semi-infinite slab of thickness t shown in Fig. 20. Let $f(R,z)$ be the probability that a nucleon decaying isotropically at a depth z, will produce in the region of the detector, a decay product, which has traversed a distance $\leq R$ in the slab.

Then

$$f(R,z)=\frac{1}{4\pi}\int_0^\alpha d\Omega=\frac{1}{2}\left(1-\frac{z}{R}\right). \qquad \text{(I1)}$$

R will be chosen so as to include only those particles with sufficient energy to exceed the lower energy gates of the detector electronics. R, so defined, is here referred to as the range of the decay product.

If we now let ρ be the density of nucleons (neutrons or protons), then for $R\geq t$, the effective number of

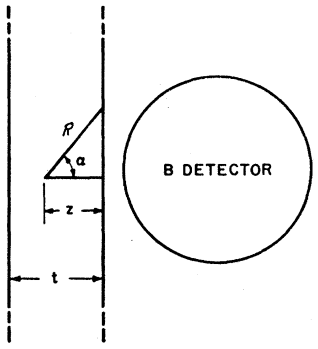

FIG. 20. Geometry used to calculate the effective number of nucleons per unit area in a semi-infinite slab.

nucleons per unit area N/A which is capable of producing detectable decay products is given by

$$\frac{N}{A}=\int_0^t f(R,z)\rho dz$$

or

$$\frac{N}{A}=\frac{\rho t}{2}\left(1-\frac{t}{2R}\right) \quad t<R. \qquad \text{(I2a)}$$

Since $f(R,z)$ is zero for $z>R$, N/A, in the case for which $t\geq R$, is obtained from (I2a) with t replaced by R.

$$N/A=\tfrac{1}{4}\rho R \quad t\geq R. \qquad \text{(I2b)}$$

APPENDIX II: PARTICLE RANGES

A. Electrons

Average electron ranges in Fe and NaCl were calculated from the formula[18]

$$R(E_0)=x_0\,(\ln 2)\,\ln\left\{\frac{E_0}{E_c\ln 2}+1\right\}, \qquad \text{(II1)}$$

where E_0 is the initial electron energy (MeV), E_c is the critical energy (MeV) and x_0 is the radiation length. This formula gives the average range of an individual electron, and is not concerned with the effects of the electron's progeny. Since the ranges of such photons could, as is predicted by the simplest of shower theories, be larger than that calculated for the electron, the use of the formula is conservative.

The above formula is based on a Monte Carlo calculation of shower production and neglects multiple scattering. In NaCl and Fe this effect is small.

The radiation length (g/cm^2) for NaCl was calculated from the formula[19]

$$1/x_0=4(N_0/A)Z(Z+1.3)(5.79\times10^{-28}\text{ cm}^2)\times\ln\{183/Z^{1/3}\}, \qquad \text{(II2)}$$

where N_0 is Avogadro's number. The critical energy for NaCl was taken as equal to that of Al which has approximately the same value of Z/A.

In calculating electron ranges in the scintillator, shower phenomena have been neglected, and minimum ionization energies have been assumed. Neglecting shower phenomena is reasonable since the radiation length ($\sim$40 cm) is comparable with the dimensions of the inner detector. The assumption of minimum ionization energies is consistent with the conservative nature of the calculation since it gives the smallest possible effective number of nucleons.

B. Photons

It will be assumed that an average photon of energy E_0 travels a distance x_0 ln2 and then produces an electron pair, each of energy $E_0/2$. The above comments concerning electron ranges in Fe and NaCl can then be applied.

In the case of photons produced in the scintillator, it is reasonable to assume that the photon does not interact prior to leaving the detector.

C. Heavy Particles

Ranges for particles heavier than electrons were obtained from various published sources.[20–22] Ranges in NaCl are taken as equal to those in Al (g/cm^2) since their values of Z/A are similar.

---

[18] R. R. Wilson, Phys. Rev. 84, 100 (1951).

[19] R. M. Sternheimer, in *Methods of Experimental Physics*, edited by L. C. L. Yuan and C. Wu (Academic Press Inc., New York, 1961), Vol. 5, Part A, Chap. 1, p. 59.

[20] B. Rossi, *High-Energy Particles* (Prentice-Hall, Inc., New York, 1952), Chap. 2, p. 44.

[21] J. H. Atkinson, Jr. and Beverly Hill Willis, University of California Lawrence Radiation Laboratory Report UCRL 2426 Rev., Vol. II, 1957 (unpublished).

[22] W. S. C. Williams and I. F. Corbett, in High Energy and Nuclear Physics Data Handbook, edited by W. Galbraith and W. S. C. Williams (National Institute for Research in Nuclear Science, Rutherford High Energy Laboratory Chilton, 1963, unpublished).